© 2017 by The American Society for Biochemistry and Molecular Biology, Inc.
This paper is available on line at http://www.mcponline.org

New Quantitative Mass Spectrometry Approaches Reveal Different ADP-ribosylation Phases Dependent On the Levels of Oxidative Stress*[S]

Vera Bilan‡§, Nathalie Selevsek¶, Hans A. V. Kistemaker‖, Jeannette Abplanalp‡§, Roxane Feurer‡, Dmitri V. Filippov‖, and Michael O. Hottiger‡**

Oxidative stress is a potent inducer of protein ADP-ribosylation. Although individual oxidative stress-induced ADP-ribosylated proteins have been identified, it is so far not clear to which extent different degrees of stress severity quantitatively and qualitatively alter ADP-ribosylation. Here, we investigated both quantitative and qualitative changes of the hydrogen peroxide (H_2O_2)-induced ADP-ribosylome using a label-free shotgun quantification and a parallel reaction monitoring (PRM) mass spectrometry approach for a selected number of identified ADP-ribosylated peptides. Although the major part of the basal HeLa ADP-ribosylome remained unchanged upon all tested H_2O_2 concentrations, some selected peptides change the extent of ADP-ribosylation depending on the degree of the applied oxidative stress. Low oxidative stress (*i.e.* 4 μM and 16 μM H_2O_2) caused a reduction in ADP-ribosylation of modified proteins detected under untreated conditions. In contrast, mid to strong oxidative stress (62 μM to 1 mM H_2O_2) induced a significant increase in ADP-ribosylation of oxidative stress-targeted proteins. The application of the PRM approach to SKOV3 and A2780, ovarian cancer cells displaying different sensitivities to PARP inhibitors, revealed that the basal and the H_2O_2-induced ADP-ribosylomes of SKOV3 and A2780 differed significantly and that the sensitivity to PARP inhibitors correlated with the level of ARTD1 expression in these cells. Overall, this new PRM-MS approach has proven to be sensitive in monitoring alterations of the ADP-ribosylome and has revealed unexpected alterations in proteins ADP-ribosylation depending on the degree of oxidative stress. ***Molecular & Cellular Proteomics 16: 10.1074/mcp.O116.065623, 949–958, 2017.***

ADP-ribosylation of proteins is a reversible post-translational modification (PTM)[1] in which the ADP-ribose moiety of NAD^+ is transferred onto a specific amino acid of the acceptor protein. Intracellular ADP-ribosylation is catalyzed by diphtheria toxin-like ADP-ribosyltransferases consisting of 17 members in humans (ARTDs, also known as PARPs) (1). Whereas many ARTDs catalyze mono-ADP-ribosylation (MARylation), only ARTD1, ARTD2, ARTD5, and ARTD6 can extend MAR by attaching additional ADP-ribose units and producing poly-ADP-ribosylation (PAR) chains (2). Under steady state conditions, PAR levels are low and hardly detectable (3). The induction of PAR synthesis occurs in response to different stress stimuli such as oxidative stress, DNA damage, and ionizing radiation and is mainly ARTD1 dependent (3). Treatment of cells with hydrogen peroxide (H_2O_2), which mimics oxidative stress in cells, induces the PLC/IP3R/Ca^{2+}/PKCα signaling cascade to subsequently activate nuclear ARTDs (mainly ARTD1) and to induce within a few minutes PAR formation in the nucleus (4, 5). The half-life of PARylation is short, and the polymers are quickly degraded by poly (ADP-ribose) glycohydrolase (PARG).

Cellular ADP-ribosylation has been linked to the development of neurodegenerative (6, 7) and metabolic diseases,

From the ‡Department of Molecular Mechanisms of Disease, University of Zurich, Winterthurerstrasse 190, CH-8057 Zurich, Switzerland; §Molecular Life Science (MLS) program of the Life Science Zurich Graduate School, University of Zurich, Winterthurerstrasse 190, CH-8057 Zurich, Switzerland; ¶Functional Genomics Center Zurich, University of Zurich/ETH Zurich, Winterthurerstrasse 190, CH-8057 Zurich, Switzerland; ‖Leiden Institute of Chemistry, Department of Bio-organic Synthesis, Leiden University, Einsteinweg 55, 2333 CC, Leiden, The Netherlands

Received November 16, 2016, and in revised form, March 20, 2017
Published, MCP Papers in Press, March 21, 2017, DOI 10.1074/mcp.O116.065623
Author contributions: V.B. and N.S. planned the experiments. V.B. performed the experiments, analyzed and interpreted the results and wrote the manuscript. H.A.V.K. and D.V.F. performed synthesis of the peptides. R.F. performed pull-down experiments with the peptides, J.A. performed the detection of oxidative stress markers by Western Blot. M.O.H. supervised the experiments and provided overall guidance.

[1] The abbreviations used are: PTM, post-translational modification; PRM-MS, parallel reaction monitoring mass spectrometry; ARTD, ADP-ribosyltransferase diphtheria toxin-like; PAR, poly-ADP-ribose; MAR, mono-ADP-ribose; AUC, area under the curve; ER, endoplasmic reticulum; PARPi, ADP-ribosylation inhibitor; LFQ, label free quantification; PARylation, reaction of PAR synthesis; MARylation, reaction of attachment of MAR to the target protein; AGC, automated gain control; PARG, poly (ADP-ribose) glycohydrolase.

Downloaded from https://www.mcponline.org by guest on November 12, 2019

inflammation (8), and tumorigenesis (9). Given the role of PARylation in various cellular processes such as the genotoxic stress response and the identification of ARTD1 as an important regulator of nuclear chromatin associated ADP-ribosylation, ARTD1 is an interesting cellular target for pharmacological interventions. Based on two seminal papers, which provided evidence that inhibitors of ADP-ribosylation (*i.e.* PARP inhibitors, PARPi) can kill tumor cells deficient for BRCA1-regulated homologous recombination (10, 11), several PARP inhibitors have been tested in clinical studies mainly for the treatment of BRCA1- and BRCA2-deficient cancer types (12). After succeeding in clinical studies, the third generation of PARPi was recently approved for the treatment of specific types of ovarian and prostate cancer (13). However, the response to PARPi treatment is difficult to predict based on the cancer cells' BRCA status only. Indeed, some BRCA-proficient tumors with other mutations have been described to be sensitive to PARPi, whereas some BRCA-deficient tumors appear resistant to PARP inhibitor treatment (14). Thus, understanding the functional role of PARylation and identifying proteins and their quantitative changes that are ADP-ribosylated under different stress conditions would represent a major step forward toward effectively predicting potential PARPi treatment outcomes in patients.

Recently, Martello *et al.* developed a MS-based method to quantify PAR chains from cells and tissues and reported that PAR chain length increased proportionally to the level of oxidative stress applied to the cells (15). However, this method does not allow the identification of the modified proteins and their acceptor sites. The recently developed ADP-ribosylation specific enrichment methods in combination with MS/MS analysis overcame this hurdle and allowed the identification of the cellular ADP-ribosylome under various stress conditions including oxidative stress (16–18). Although the H_2O_2-induced ADP-ribosylome has been characterized (16–18), it is still not clear whether the numbers of ADP-ribosylated molecules and/or modified sites of a given protein vary with stress intensity. Understanding the quantitative and qualitative changes of protein ADP-ribosylation will provide valuable insights into stress signaling events and reveal the functional importance of ADP-ribosylation during oxidative stress.

The development of targeted proteomics methods significantly improved MS-based quantification of proteins (19, 20). Selected reaction monitoring (SRM) as well as parallel reaction monitoring (PRM) provide exceptional sensitivity and reproducibility in comparison to shotgun measurements (21, 22). In a targeted method, the MS instrument selects a set of precursor ions with a defined *m/z* from MS1 for subsequent fragmentation in the collision cell and the resulting fragment ions are used for protein quantification. Typically, 50 to 100 proteins can be measured in one single MS run (20, 23). The high sensitivity and reproducibility of PRM measurements were already successfully applied to study various PTMs (24–26), *e.g.* ubiquitination even without an enrichment step (27).

Here, we report both quantitative and qualitative changes of protein ADP-ribosylation in cells exposed to non-lethal oxidative stress by using both shotgun and specifically developed PRM approaches for the analysis of selected ADP-ribosylated acceptor sites induced by oxidative stress.

EXPERIMENTAL PROCEDURES

Experimental Design and Statistical Rationale—The study aimed to define the quantitative and qualitative levels of ADP-ribosylation under various degrees of oxidative stress. HeLa cells were used as a model system to determine a basal and oxidative stress-induced ADP-ribosylome. Label-free quantification (LFQ) and PRM were used to analyze quantitative changes of ADP-ribosylated peptides. The ADP-ribosylated H2B-like standard peptide was used as an internal control to evaluate the variability between measurements. The PRM method reproducibility was controlled by a technical triplicate of a 250 μM H_2O_2-treated HeLa sample, which was divided into three parts and enriched in parallel (see Supplementary material, supplemental Fig. S1). This control experiment revealed a high reproducibility of the PRM method (CV = 0.059). All further quantitative PRM experiments were performed in biological duplicates. The different samples were tested for significant differences by using an ANOVA test comparing oxidative stress-induced samples to each other and to an untreated control. Only changes > 2-fold were further considered.

Cell Culture—HeLa cells were cultured in DMEM (GIBCO, Thermo Fisher Scientific, Waltham, MA) (substituted with 10% FCS and penicillin/streptomycin) at 37 °C and 5% CO_2. SKOV3 and A2780 were grown in RPMI1640 (supplemented with 10% FCS and 1% penicillin/streptomycin) at 37 °C and 5% CO_2.

Synthesis of H2B-like Standard ADP-ribosylated Peptide—The synthesis of the peptide was described in (28). The schematic chemical structure of the peptide can be found in supplemental Fig. S1*A* and has the following sequence: Acetyl-Pro-Gln(ADPr)-Pro-Ala-Lys-Ser-Ala-Pro-Ala-Pro-Lys-Lys-Gly-NH_2. The non-modified peptide was synthesized as described in (28) and has the following sequence: Acetyl-Pro-Gln-Pro-Ala-Lys-Ser-Ala-Pro-Ala-Pro-Lys-Lys-Gly-NH_2.

Enrichment of ADP-ribosylated Peptides from HeLa Cell Lysate—To induce PAR formation, cells were treated with various concentrations of H_2O_2 for 10 min and lysed in lysis buffer (50 mM Tris pH 8, 1% Nonidet P-40, 400 mM NaCl, 1 mM EDTA, 0.1% sodium deoxycholate, complete protease inhibitor mixture (Roche, Mannheim, Germany), 10 μM PJ34, 75 μM tannic acid). After lysis and acetone precipitation, extracted proteins were digested with trypsin (cleaves C-terminal to arginine and lysine, Promega, Madison, WI) and the obtained peptide mixture enriched as described (18) with the following modifications. The total protein lysate concentration used for each enrichment was 20 mg for shotgun and 5 mg for PRM measurements. 100 ng of the ADP-ribosylated H2B-like standard peptide was spiked into the samples used for quantitative studies before the Af1521 pulldown. The binding of the H2B-like standard peptide to Af1521 was validated with SDS-PAGE and Western blot analysis (supplemental Fig. S1 and supplementary Methods).

Immunofluorescence—Immunofluorescence staining for PAR was performed as described in Weber *et al.* (2013) using a homemade 10H anti-PAR antibody. Oxidative stress was induced by H_2O_2 treatment for 10 min (unless otherwise indicated) at the indicated concentrations in PBS, 1 mM $MgCl_2$. The images were taken using a Leica DMI 6000B microscope and processed with ImageJ software (v. 1.6.0).

Liquid Chromatography and Mass Spectrometry Analysis—Mass spectrometry analysis was performed on an Orbitrap Q Exactive HF mass spectrometer (Thermo Fisher Scientific) coupled to a nano EasyLC 1000 (Thermo Fisher Scientific). The peptides were loaded

Downloaded from https://www.mcponline.org by guest on November 12, 2019

onto a self-made column (75 μm $\times$ 150 mm) which was packed with reverse-phase C18 material (ReproSil-Pur 120 C18-AQ, 1.9 μm, Dr. Maisch GmbH) and connected to an empty Picotip emitter (New Objective, Woburn, MA). The peptides were separated at a flow rate of 300 nL/min by a gradient from 2 to 25% B in 90 min. Solvent composition at the channels A and B was 0.1% formic acid and 0.1% formic acid, 99.9% acetonitrile, respectively.

To perform shotgun measurements, the mass spectrometer was set to acquire full-scan MS spectra (300–1700 *m/z*) at a resolution of 60,000 after accumulation to an automated gain control (AGC) target value of 3×10^6. Charge state screening was enabled, and unassigned charge states, and single charged precursors were excluded. Ions were isolated using a quadrupole mass filter with a 2 *m/z* isolation window. A maximum injection time of 110 ms was set. HCD fragmentation was performed at a normalized collision energy (NCE) of 28%. Selected ions were dynamically excluded for 20 s.

For PRM measurements, the Q Exactive HF was set to perform MS1 scans (350–1000 *m/z*) followed by 12 MS/MS acquisitions in PRM mode. HCD fragmentation was conducted at a normalized collision energy (NCE) of 28%. The full MS scan was carried out with an AGC target of 10^5 and at a 60,000 resolution. Maximum injection time was set to 110 ms. The subsequent PRM MS/MS scans were performed with an AGC target of 3×10^6 and at a 60′000 resolution with an isolation window of 2 *m/z*. Maximum injection time was set to 15 ms. PRM measurements were performed in a time scheduled mode. The isolation lists for each performed method can be found in supplemental Tables S3, S4, and S5.

Shotgun Data Analysis—The raw file processing and the database search using Mascot were conducted as described in (30) with further indicated modifications. Briefly, MS and MS/MS spectra were converted to Mascot generic format (MGF) using Proteome Discoverer, v2.1 (Thermo Fisher Scientific). The MGFs were searched against the UniProtKB human database (taxonomy 9606, version 20140422), which included 35787 Swiss-Prot, 37802 TrEMBL entries, 73589 decoy hits, and 260 common contaminants. Mascot 2.5.1.3 (Matrix Science) was used for peptide sequence identification using previously described search settings. Briefly, peptide tolerance was set to 10 ppm and the MS/MS tolerance to 0.05 Da. False discovery rates at the peptide and protein level were analyzed with decoy hits. Enzyme specificity was set to trypsin and up to four missed cleavages were allowed. The following modifications were searched: carbamidomethylation (C, fixed), oxidation (M, variable), ADP-ribosylation (K, R, D, E, variable). A Mascot score >20 and an expectation value <0.05 were considered to identify the correctly assigned peptides. The ADP-ribosylation sites with a site localization confidence of $\geqq$95% were considered as correctly assigned (31).

Progenesis QI software (Nonlinear Dynamics, Purham, NC) was used to perform label-free quantification based on the MS1 precursor peak area. Raw data were imported into the Progenesis QI (v. 3.0.6039.34628) and aligned based on the MS1 peak retention time. All samples were normalized based on the total signal intensity to account for sample loading variations. The obtained results were exported as MGF and searched with Mascot as indicated above. The Mascot search results were imported into Scaffold software (v.4.7.2) and filtered for protein and peptide FDR values of 0.01. When multiple precursors were observed for the same peptide, the values were summed up to obtain the total level of the peptide.

PRM Data Analysis Using Skyline—The acquired PRM raw files were imported into Skyline daily (v.3.5.1.9942). ADP-ribosylation was defined as $H_{21}C_{15}N_5O_{13}P_2$ with 249.0862 and 347.0631 neutral losses for K, R, D, E, and Q. For each targeted peptide, the precursor and the 5 most intense fragment ions were monitored and used for quantification.

The mProphet algorithm was used for automatic peak picking. The second best peak model was trained using samples treated with 64 μM of H_2O_2. The Q value was set to 0.1. Peaks were manually checked for correct integration. The peaks that were automatically assigned for >60% samples were considered as correctly identified, the wrongly assigned peaks in these cases were integrated manually using the corresponding retention times and the relative fragment ions intensity from the library. The area under the curve (AUCs) of each transition was summed up to obtain the AUCs of the peptide. When several precursors were monitored for one peptide, the AUCs of these precursors were summed up.

To evaluate protein abundance changes in ovarian cancer cell lines, 5 unique tryptic peptides with no miscleavages and carrying no variable modifications were selected from the SRM Atlas (http://www.srmatlas.org). The SWATH Atlas (32) was used to obtain the fragmentation information and retention time for each peptide. The peptides with no library hits were excluded from the analysis. The statistical data analysis was performed with the R package "R for Proteomics" using R studio (v.0.99.903, R (v 3.2.4)) and using the Perseus software (v.1.5.5.3). GO analysis (cellular localization) was determined using the UniProt protein name and the CellWhere application (http://cellwheremyology.rhcloud.com).

Data Deposit—All MS raw files and Scaffold files presented in this study can be accessed at MassIVE (MSV000080334, ftp://massive.ucsd.edu/MSV000080334)

RESULTS

H_2O_2 dose-dependent PAR formation reaches maximum levels at 10 min in HeLa cells—To gain more molecular insights into PAR formation and to identify the time for maximal PAR formation in cells, HeLa cells were treated with 1 mM H_2O_2 for four different time points (0, 10, 15, 30 min) and PAR induction was analyzed via immunofluorescence with 10H PAR antibody (supplemental Fig. S2*A*). As the H_2O_2-induced ADP-ribosylome of HeLa cells was successfully identified without the need of a PARG knockdown (17, 18), we used these cells as a model system to better understand the quantitative changes of protein ADP-ribosylation following oxidative stress. The maximal PAR signal was detected after 10 min H_2O_2 treatment (supplemental Fig. *S2A*). To confirm this result we quantified the modification dynamics of specific ADP-ribosylated peptides in HeLa cells treated with 500 μM H_2O_2 for 0, 5, 10, 30, 60 min using a SILAC MS approach (supplemental Fig. *S2B*) (18). These experiments confirmed that the highest level of ADP-ribosylation in HeLa cells is at 10 min. We thus performed all following experiments at this time point.

To determine whether the observed cellular ADP-ribosylation is concentration-dependent, PAR formation was monitored in HeLa cells treated for 10 min with increasing concentrations of H_2O_2 (0, 62.5, 250 μM, and 1 mM). PAR-specific immunofluorescence was observed for all tested H_2O_2 concentrations, although the PAR signal intensity steadily increased with the applied concentration of H_2O_2 (supplemental Fig. S2*C*). The differential PAR signal intensities could result from (i) increased PAR chain length of previously modified proteins, (ii) increased *de novo* ADP-ribosylation of previously unmodified protein types, or (iii) an increase in the number of ADP-ribosylated molecules belonging to a previously already

Downloaded from https://www.mcponline.org by guest on November 12, 2019

modified protein type (supplemental Fig. S2*D*). Martello *et al.* observed previously a similar correlation between PAR chain length measured by LC-MS/MS and the level of oxidative stress, indicating that the observed changes in signal intensities can be at least partially explained by the growth of PAR chains (15). However, these results and the limitations of the here performed immunofluorescence analysis with the 10H PAR antibody, which only binds PAR chains containing at least 3–4 ADP-ribose units (33), do not allow addressing potential changes of the ADP-ribose acceptor sites (scenarios ii and iii).

The H_2O_2-induced Changes in the ADP-ribosylome Remain Qualitatively Stable With Increasing H_2O_2 Concentrations—To investigate whether different degrees of oxidative stress would induce qualitatively different ADP-ribosylomes (*i.e.* severity dependent ADP-ribosylation) HeLa cells were left either untreated or treated with increasing concentrations of H_2O_2 (62 μM, 250 μM, and 1 mM; $n = 3$). Cells were subsequently lysed in presence of PARP and PARG inhibitors to avoid lysis induced ADP-ribosylation. The ADP-ribosylated peptides were enriched using the Af1521 macrodomain and proteins were identified by shotgun MS analysis (18). Although untreated HeLa cells showed no detectable PAR signal by immunofluorescence (supplemental Fig. S2*A* and S2*C*), the shotgun MS approach identified 25 ADP-ribosylated proteins (Fig. 1*A*), suggesting that already in untreated cells proteins are ADP-ribosylated. To test whether the basal ADP-ribosylome was dependent on ARTDs, we repeated the analysis of untreated cells including the cells which were pretreated before cell lysis for 30 min with PARPi PJ34, which mainly inhibits PARylation (34). The shotgun MS analysis of H_2O_2 untreated but PJ34 pre-treated HeLa cells ($n = 2$) revealed that 9 ADP-ribosylated proteins remained ADP-ribosylated despite PARPi PJ34 in HeLa cell extracts.

Next, we compared the ADP-ribosylomes identified in cells treated with different H_2O_2 concentrations (62 μM, 250 μM, and 1 mM) to the untreated control and between each other. Overall, treatment of HeLa cells with H_2O_2 increased the number of identified ADP-ribosylated peptides when compared with untreated HeLa cells (Fig. 1*A*, 1*B*, and supplemental Table S1). In total, 83 proteins and 169 sites carrying ADP-ribose were identified using our shotgun MS approach following treatment with H_2O_2. When comparing the ADP-ribosylomes induced by different H_2O_2 concentrations, the overlap of identical modified proteins was 52% (*i.e.* observed for at least two H_2O_2 concentrations, Fig. 1*A*). Considering the moderate reproducibility of shotgun MS measurements, which usually peaks at 60% (35), we concluded that the observed H_2O_2-induced ADP-ribosylome sample variation (with 52% overlap) does not vary substantially, suggesting that the numbers of H_2O_2-induced ADP-ribosylation sites do not change upon different severities of oxidative stress (Fig. 1*B*).

The H_2O_2-induced ADP-ribosylome Does Not Quantitatively Change at Mid and High H_2O_2 Concentrations—Our shotgun MS experiment revealed that H_2O_2 treatment of HeLa cells induces qualitatively comparable ADP-ribosylomes. To understand if the dose-dependent induction of ADP-ribosylation signal observed by immunofluorescence following H_2O_2 stress was caused by a gradually increased number of ADP-ribosylated molecules of a given protein (*i.e.* quantitative level of ADP-ribosylation; scenario ii at supplemental Fig. S2*D*) in HeLa cells, we performed label-free quantification (LFQ) on our shotgun samples (HeLa treated with 0–1 mM H_2O_2). In total, 83 different proteins with 128 unique ADP-ribose acceptor sites were reliably quantified across all samples (Fig. 1*C*, supplemental Table S2). By comparing the MS1 intensities of ADP-ribosylated peptides between the different H_2O_2 concentrations and untreated cells, two groups of ADP-ribosylated proteins were identified.

The first group contained 55 proteins comprising 82 ADP-ribose acceptor sites that were already modified under untreated (basal) conditions and did not significantly change with increasing H_2O_2 concentrations (Fig. 1*C* and 1*D*, stable) Many of these identified proteins were already identified in untreated HeLa cells with the shotgun approach (Fig. 1*A*, 1*C*, and 1*D*). Although some proteins, like H2B histone variants and ARTD1, showed a tendency of increased ADP-ribosylation, the ADP-ribosylation status of these proteins was not significantly regulated by H_2O_2 signaling.

The second group contained 38 proteins comprising 46 ADP-ribose acceptor sites, that under basal conditions were only to a minor part already ADP-ribosylated, but showed a quantitative increase of ADP-ribosylation starting at 62 μM H_2O_2, and increased although not significantly until 250 μM H_2O_2 to reach a plateau (Fig. 1*C* and 1*E*). This group contained nuclear proteins, including already known ADP-ribosylation targets like YY1, TOP1, and CTCF. Although the ADP-ribosylation of these proteins was H_2O_2-dependent (significantly induced comparing untreated to 62 μM H_2O_2), there was no further significant quantitative increase in the amount of detectable modified peptides when cells were treated with higher concentrations of H_2O_2 (Fig. 1*C* and 1*E*), indicating that already at 62 μM H_2O_2 the oxidative-induced ADP-ribosylome is established. This data therefore provides strong evidence that the observed increase in the PAR signal by immunofluorescence was mainly the result of PAR elongation rather than an increase in the number of modified proteins.

Protein ADP-ribosylation Required At Least Mid H_2O_2 Concentration—Martello *et al.*, detected PAR formation starting at a minimal concentration of 10 μM H_2O_2 (15). We thus repeated our immunofluorescence analysis in HeLa cells using 4 μM and 16 μM H_2O_2 (*i.e.* mild conditions). Although 16 μM H_2O_2 induced a weak, but detectable PAR formation, PAR formation with 4 μM H_2O_2 was hardly detectable, indicating that the extent of PARylation is neglectable under these conditions (Fig. 2*A*). However, the activation of cellular oxidative stress signaling was already occurring at these low concentrations of H_2O_2 as shown by the detection of stress markers such as p-ERK1/2 or p-p38 (supplemental Fig. S3*A*).

Downloaded from https://www.mcponline.org by guest on November 12, 2019

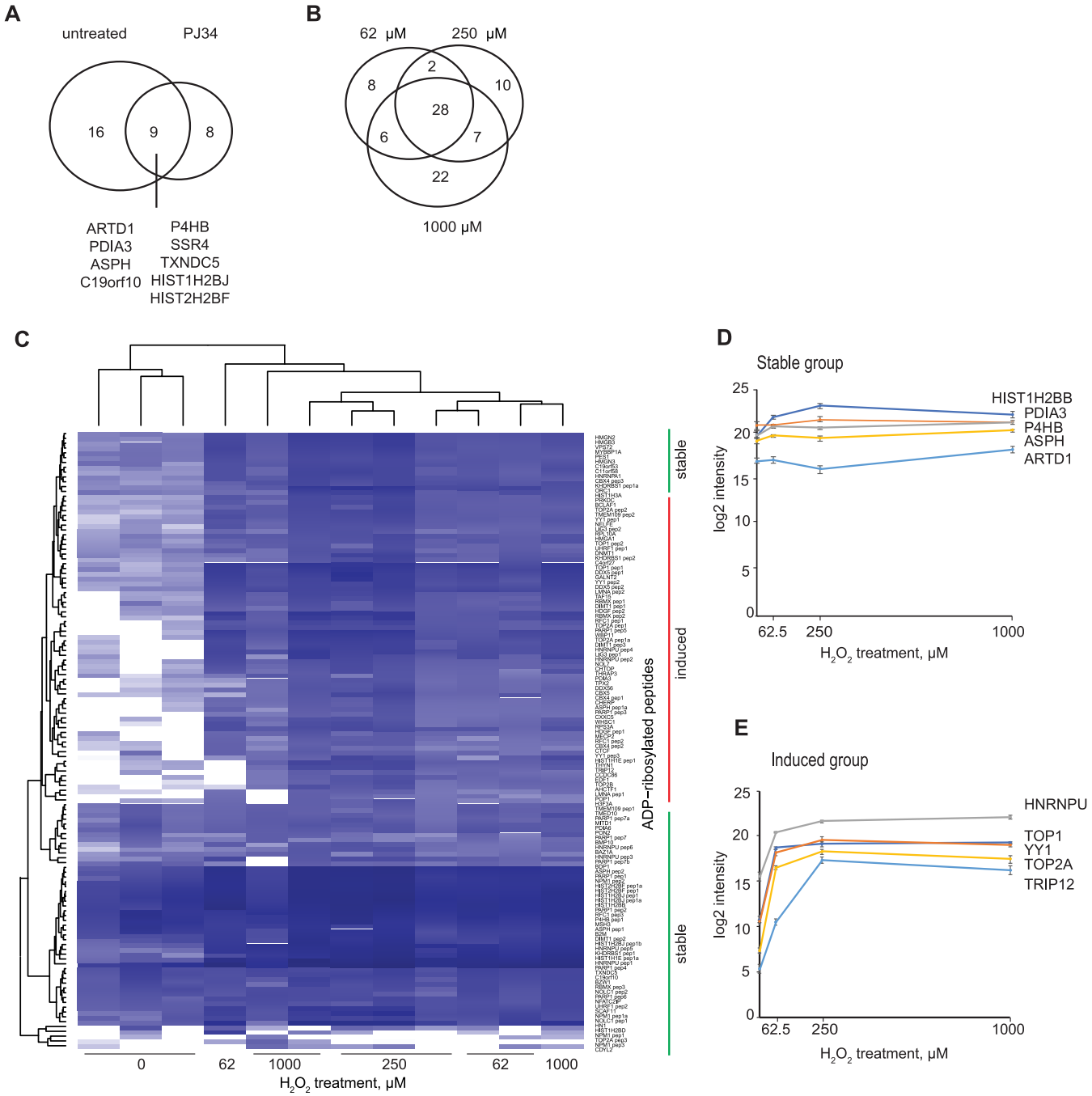

FIG. 1. **Quantification of the oxidative stress-induced HeLa ADP-ribosylome identified two groups of ADP-ribosylation changes.** *A*, The Venn diagram shows the overlap between the ADP-ribosylated proteins of HeLa cells under untreated ($n = 5$) and PJ34 pre-treated ($n = 2$) conditions. The identification was performed by shotgun measurements. *B,* The Venn diagram shows the overlap between the HeLa samples treated with indicated concentrations of H_2O_2 ($n = 3$) identified by shotgun. *C*, The heatmap represents the changes in ADP-ribosylated peptides in HeLa cells exposed to the indicated concentrations of H_2O_2 detected using LFQ MS measurement ($n = 3$). The identified ADP-ribosylome was divided into two groups ('stable' and 'induced', shown on the right with vertical lines) based on the differences between H_2O_2-treated and untreated samples. The induced group contained proteins that showed a significant up-regulation of ADP-ribosylation upon H_2O_2 treatment with the lowest tested dose (62 μM *versus* untreated, ANOVA, $p < 0.05$). The values were log2 transformed. *D*, Examples of quantitative changes of ADP-ribosylated proteins from the stable group. The average of three measurements and standard deviations after log2 transformation are shown. *E*, Examples of quantitative changes of ADP-ribosylated proteins from the induced group. The average of three measurements and standard deviations after log2 transformation are shown.

Downloaded from https://www.mcponline.org by guest on November 12, 2019

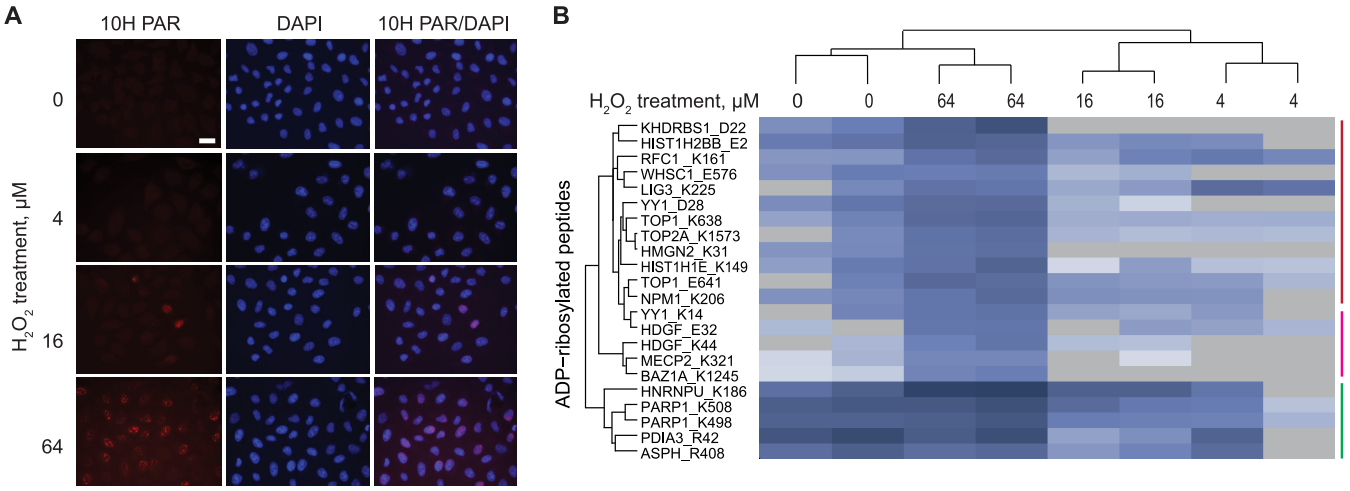

FIG. 2. **Significantly regulated ADP-ribosylated peptides in HeLa cells treated with low dose of H_2O_2 (4–64 µM).** *A*, Immunofluorescence analysis of HeLa cells treated for 10 min with the indicated concentrations of H_2O_2. Cells were stained with DAPI and PAR 10H antibody. Scale bars: 25 µm. *B*, The heatmap shows the significantly regulated ADP-ribosylated sites of HeLa cells at a low dose of oxidative stress detected using PRM MS measurement (ANOVA, $p < 0.05$). The colored vertical lines indicate the "stable" (green) and "reduced" (red) groups of ADP-ribosylated proteins ($n = 2$). The values were log2 transformed.

To ensure reliable and reproducible measurements of protein ADP-ribosylation across the samples, and to increase the sensitivity of the measurements (21), we developed a targeted MS-based method for defined protein ADP-ribosylation based on a PRM approach. The protein candidates were selected from our LFQ measurements and included 71 proteins (133 ADP-ribose acceptor sites). After assay development (see supplementary Information), our PRM method targeted 66 proteins and 113 ADP-ribose acceptor sites (see supplemental Table S3 for PRM method).

Next we preformed PRM measurements on ADP-ribosylated peptides enriched from HeLa cells exposed to 4 µM, 16 µM and 64 µM H_2O_2. To monitor the efficiency of the enrichment workflow, we added a standard H2B-like ADP-ribosylated peptide (supplemental Fig. S1) in each protein isolate that we monitored by PRM. In total, we reliably quantified 47 proteins with 60 ADP-ribosylated peptides. Based on the measured quantitative ADP-ribosylation changes, the analyzed peptides clustered into three groups (Fig. 2*B* and supplemental Fig. S3*B* and S3*C*). The first group included 9 proteins with 13 ADP-ribosylated peptides, which were already strongly ADP-ribosylated under basal conditions and remained modified for all the H_2O_2 concentrations tested (*e.g.* ARTD1 and PDIA3; compare with Fig. 1*A*). Some proteins in this group showed a trend of reducing ADP-ribosylation states at 4 and 16 µM H_2O_2, but reaching the levels observed under untreated conditions at 64 µM H_2O_2. Histone H2B variants were among these proteins. This group also contained PDIA3 and P4HB (also known as PDIA6), the ER proteins that are stably modified in untreated cells and were identified to maintain their ADP-ribosylation level in our LFQ measurements (Fig. 2*B*).

The second group contained 17 proteins with 23 ADP-ribosylated peptides and at first resembled the first group in their ADP-ribosylation profile (*i.e.* was detectable under basal conditions, and reduced at 4 µM or 16 µM H_2O_2), but was strongly induced at 64 µM H_2O_2 (Fig. 2*B* and supplemental Fig. S3*B* and S3*C*). Proteins belonging to the third group (26 proteins with 26 ADP-ribose acceptor sites) were not ADP-ribosylated under untreated conditions or at low H_2O_2 concentrations (4 µM or 16 µM), but showed robust ADP-ribosylation at 64 µM H_2O_2 (*e.g.* MECP2, BAZ1A, HDGF). GO analysis revealed that this group is significantly ($p = 0.0132$) enriched for proteins with chromatin and transcription factor binding capacities. Five of the identified proteins (*e.g.* MECP2 and CTCF) act as transcriptional co-repressors. The robust induction of ADP-ribosylation only at 64 µM H_2O_2 suggests that for the modification of proteins in group 2 and 3 a certain level of oxidative stress is required (supplemental Fig. S3*B*). We validated the results by preparing an additional biological replicate, and the results were comparable to the first measurement (supplemental Fig. S3*D*).

The Basal and H_2O_2-induced ADP-ribosylomes of SKOV3 and A2780 Differ—Next, we applied our newly developed PRM method to two pathophysiologically relevant ovarian cancer cell types SKOV3 and A2780, which have been described as PARPi-resistant and -sensitive, respectively (36). These two cell lines were treated with three different PARPi (Veliparib, Talazoparib, Olaparib) and an MTT metabolic assay was performed to confirm the reported PARPi sensitivity. Indeed, A2780 cells were found to be sensitive to lower doses of all three tested PARPi whereas higher doses were required to reduce the metabolic activity of SKOV3 cells (supplemental Fig. S4*A*).

Downloaded from https://www.mcponline.org by guest on November 12, 2019

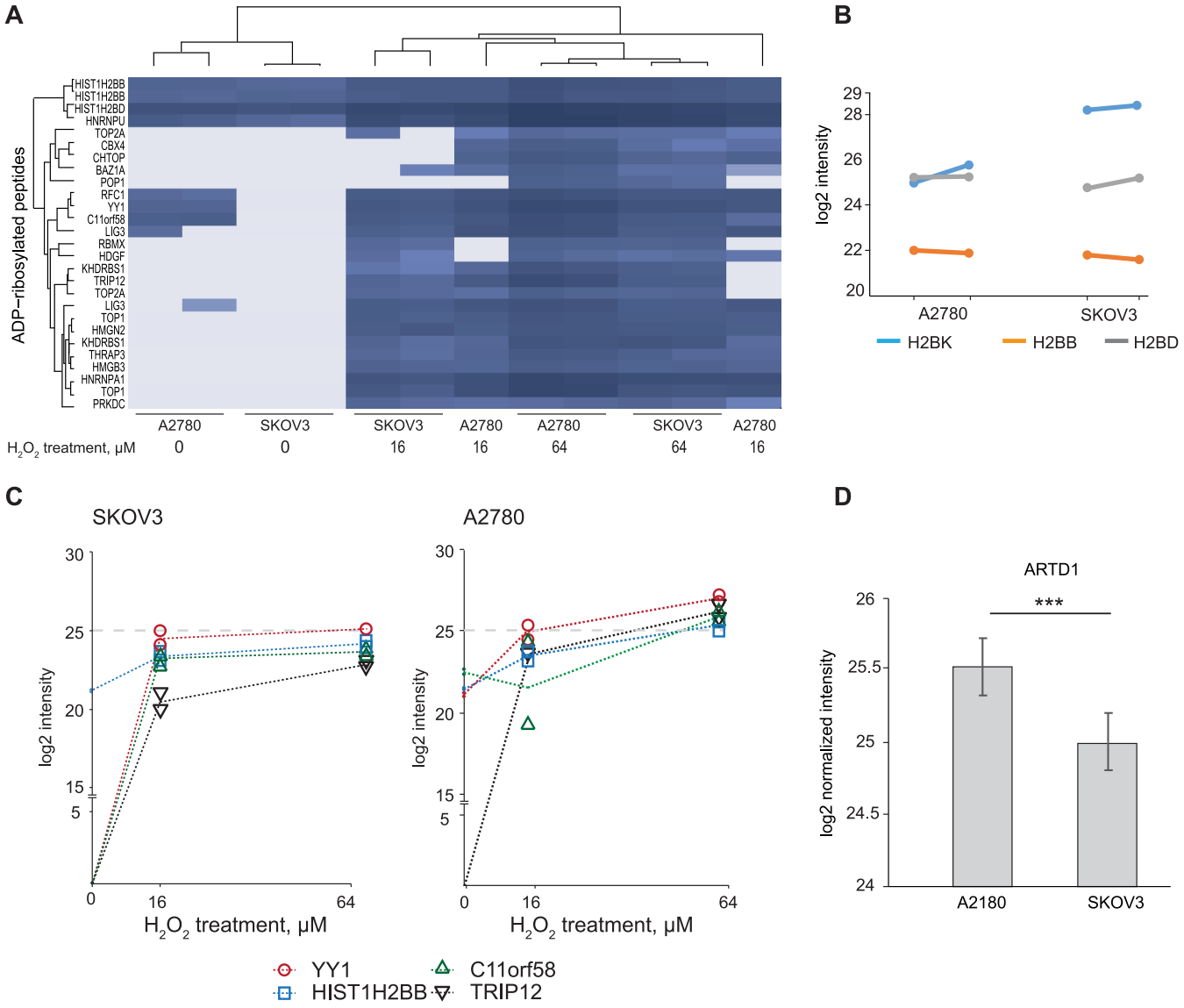

FIG. 3. **Differences in the ADP-ribosylation level in ovarian cancer cells at basal and H_2O_2-treated conditions.** A, The heatmap shows the significantly regulated ADP-ribosylated proteins in oxidative stress in two different ovarian cancer cell lines (A2780 and SKOV3) ($n = 2$, ANOVA, $p < 0.05$), detected using PRM MS measurement. The values were log2 transformed. B, The ADP-ribosylation level of H2B histone variants for SKOV3 and A2780 detected at basal/untreated condition detected using PRM MS measurement. The values were log2 transformed ($n = 2$). C, Examples of oxidative stress-induced ADP-ribosylated targets for A2780 and SKOV3 at different concentrations of H_2O_2 detected using PRM MS measurement. The values were log2 transformed and plotted separately, the dashed lines connect the average values ($n = 2$). D, The level of ARTD1 in A2780 and SKOV3 cells ($n = 6$, mean ± S.D., student t test, $p = 0.000083$), detected using PRM MS measurement.

To test whether the detectable ADP-ribosylomes in untreated and H_2O_2 treated cancer cells correlate with their differential PARPi-sensitivity (36), we analyzed the ADP-ribosylation in SKOV3 and A2780 using our PRM method (see supplemental Table S4 for PRM method) under basal and H_2O_2 treated conditions (16 μM and 64 μM; $n = 2$). Out of the 66 proteins targeted, we reliably quantified 27 proteins with 36 ADP-ribosylated peptides (Fig. 3*A* and supplemental Fig. S4*B*) under basal conditions. Although the histone H2B variants 1-B and 1-D were ADP-ribosylated at the same level under untreated conditions for SKOV3 and A2780 cells, the ADP-ribosylation state of the 1-K variant was 7.4-fold higher in SKOV3 cells (Fig. 3*B*). In addition to the identified differences in the modification states of H2B histone variants, YY1, RFC1 and C11orf58 were ADP-ribosylated in A2780 cells but not in SKOV3 cells.

Upon H_2O_2 treatment 27 ADP-ribosylated peptides (out of 36 quantified) were significantly up-regulated in both SKOV3 and A2780 cells independent of the H_2O_2 concentration used (Fig. 3*A*, ANOVA test, $p < 0.05$). Although the ADP-ribosylated peptides from A2780 showed moderate but gradual increases in their ADP-ribosylation levels in response to in-

Downloaded from https://www.mcponline.org by guest on November 12, 2019

creasing H_2O_2 concentrations, the modified proteins identified in the SKOV3 cells reached the maximum of detectable ADP-ribosylation levels already at low H_2O_2 concentrations (16 μM; Fig. 3*C*). In contrast, for 20 ADP-ribosylated peptides (17 proteins) the ADP-ribosylation levels were significantly higher in A2780 than in SKOV3 cells following 64 μM H_2O_2 treatment (ANOVA test, $p < 0.05$). In summary, we found a slightly different ADP-ribosylation pattern in response to H_2O_2 in PARPi-sensitive A2780 cells compared with PARPi-resistant SKOV3 cells (supplemental Fig. S3*C*).

The resistance to PARP inhibitors negatively correlates with the abundance of ARTD1—Potentially, the observed different levels of ADP-ribosylation could be explained by differential abundance of the analyzed proteins. Thus, we evaluated the overall abundance of the ADP-ribosylated proteins by performing PRM measurements targeting 3–5 peptides per proteins, which were found to be ADP-ribosylated in our first PRM cancer cell line measurement (see supplemental Table S5 for PRM method). This experiment revealed that the overall protein abundance was not altered and was very comparable in the tested cell lines (supplemental Fig. S4*C*) whereas, interestingly, the level of ARTD1 in SKOV3 cells was 30% lower compared with A2780 (Fig. 3*D*). Unfortunately, because of the high sequence similarities, we were unable to evaluate the abundance of the specific H2B variants.

DISCUSSION

Here, we analyzed with newly developed MS-based approaches the quantitative and qualitative changes of the cellular ADP-ribosylome in response to treatment with different H_2O_2 concentrations.

We first evaluated the qualitative characteristics of ADP-ribosylomes for different H_2O_2 concentrations, and found that the identified ADP-ribosylomes are comparable, indicating that upon H_2O_2 treatment nuclear ARTDs reproducibly modify a pre-defined set of proteins involved in the oxidative stress response. To perform the quantitative evaluation, we applied label free quantification which led to the development of an oxidative stress-tailored PRM approach. Based on the identified quantitative changes of the ADP-ribosylome, ADP-ribosylated proteins can be divided into a basal (*i.e.* H_2O_2-independent) and a H_2O_2-signaling dependent group. The basal, H_2O_2-independent group maintained its modification level with all tested H_2O_2 concentrations and contained ADP-ribosylated proteins localized to various cytoplasmic compartments. Notably, seven of the identified proteins localized to the endoplasmic reticulum (ER), among them three protein disulfide isomerases (PDIA1, 3, and 6) which were found to be ADP-ribosylated on arginines and are likely to be involved in the unfolded protein response. Interestingly, several ARTs also have been implicated in the unfolded protein response, *i.e.* ARTD15 (37) and ARTC1 (38). However, the potential writers of these and other basal ADP-ribosylated sites have to be identified and confirmed. Many of the identified ADP-ribosylation sites at basal conditions were insensitive to PJ34 pretreatment, indicating that they are either modified by PJ34 insensitive ARTs or that their erasure takes longer than 30 min (the time of PJ34 pre-treatment), thus shifting the cellular state of these ADP-ribose acceptor sites to the modified form. Under basal conditions, HeLa show no PAR staining, suggesting that the ADP-ribosylated sites detected in untreated cells are most probably MARylated. Unfortunately, because of the PARG treatment step required during the enrichment protocol, it is currently not yet possible to experimentally distinguish between PARylation or MARylation. Finally, the H_2O_2-independent group contained 35 proteins which localized to the nucleus. These proteins showed increased numbers of ADP-ribosylated peptides when treated with 64 μM H_2O_2, however, the changes were not significant. Potentially, these sites are regulated by H_2O_2, but because of either technical or biological variability failed to reach significance.

ADP-ribosylation in the second group of proteins was induced by H_2O_2 treatment and its extent was H_2O_2 concentration-dependent, although this response is more complex as expected. When HeLa cells were exposed to mid oxidative stress (*i.e.* 64 μM H_2O_2), we observed a significant increase in the quantity of ADP-ribosylated proteins compared with untreated cells. However, the numbers of modified peptides did not quantitatively change when the oxidative stress was increased further from 64 μM up to 1 mM H_2O_2. The relatively stable levels of ADP-ribosylation (quantitatively and qualitatively) indicate that upon treatment by H_2O_2 nuclear ARTDs modify only a specific set and amount of proteins.

Interestingly, low oxidative stress (*i.e.* 4 and 16 μM H_2O_2) either did not induce ADP-ribosylation (*i.e.* sites were not detected at basal condition and mild oxidative stress) or even decreased it (sites were detected under basal condition but lost the modification in mild oxidative stress), although phosphorylation of p38 could be observed under these conditions (supplemental Fig. S3*A*). There are several possible explanations for the reduction of ADP-ribosylation levels at mild oxidative stress. First, low H_2O_2 doses could induce the activity of ADP-ribose (glyco)hydrolases, e.g. PARG, that would demodify existing basal ADP-ribosylation. The enzymatic activity of this class of enzymes remains poorly understood, and further investigations are needed to substantiate this possibility. Alternatively, H_2O_2 stimulation might activate different signaling pathways, which could lead to the induction of other PTMs. In this case, the peptides might gain an additional mass shift, making them undetectable using our PRM method. At high concentration of H_2O_2, ADP-ribosylation would be strongly induced leading to the accumulation of peptides, which are predominately or exclusively ADP-ribosylated. An exception from the general down-regulation/absence of ADP-ribosylation was the detected up-regulation of LIG3 and RFC1, which are involved in DNA repair. The function of ARTD1 and PARylation to promote the genotoxic stress response is well studied (5). DNA repair proteins, *e.g.*

Downloaded from https://www.mcponline.org by guest on November 12, 2019

XRCC1, are recruited to the sites of DNA damage by binding to PAR chains (39–41). It is thus not clear, why LIG3 and RFC1 are ADP-ribosylated at mild oxidative stress.

The observed variations in the intensities of the PAR signal observed already at 10 μM H_2O_2 with LC-MS/MS for PAR (15) seems mainly because of the increased length of PAR chains on pre-MARylated proteins (scenario i) and not because of the increase of newly modified protein (*i.e. de novo* ADP-ribosylation (scenario ii) or an increased number of modified molecules of the same proteins (scenario iii, supplemental Fig. S2*D*)). At mid H_2O_2 concentration (*i.e.* 62 μM H_2O_2), induction of ADP-ribosylation according to scenario ii and iii occurs, while at high H_2O_2 concentrations (*i.e.* $>$ 250 μM H_2O_2), the increase in PAR signal is because of PAR elongation. Thus, flexible PAR elongation at low and high H_2O_2 concentrations seems to allow a faster signaling in order to precisely and quickly respond to oxidative stress. The molecular mechanism regulating the transition between the different response phases remains to be further investigated.

Overall, the presented results show that it is possible to evaluate the changes in the level of ADP-ribosylation in oxidative stress using label-free quantification and targeted PRM approaches. Moreover, the developed PRM method was used to assess the levels of ADP-ribosylation in two ovarian cancer cell lines. We noted differences already in the basal ADP-ribosylome. At basal conditions, 10 proteins (including 11 ADP-ribosylated peptides) were detected in ovarian cancer cells, including three histone H2B variants (Fig. 3*B*). In human somatic cells, 13 H2B variants with only minor amino acid differences (usually 2–5 amino acids) were identified (42). Most H2B variants have a serine-and-threonine-to-alanine (S/T-A) conversion in their sequence. Moreover, different cancer cell lines were shown to differentially express certain H2B variants (42), indicating that these variants are essential for tumorigenesis. H2B E2 modification is one of the most abundant ADP-ribosylation sites and can be already detected in untreated cells. We detected H2B to be ADP-ribosylated at position 2 in all variants. In HeLa cells, we did not observe any differences in the level of H2B variants at various degrees of oxidative stress. In the PARPi resistant cell line SKOV3, the level of H2B variant K was significantly up-regulated in comparison to A2780. The role of H2B variants and their PTMs is increasingly being studied, *e.g.* the phosphorylation of histone variant H2B3B at S36 was shown to regulate cellular stress responses (43).

The PARPi sensitive A2780 cells showed an up-regulation of several ADP-ribosylated proteins under basal conditions (*i.e.* YY1, RFC1 and C11orf58), which correlated with higher protein levels of ARTD1 in these cells. Interestingly, these ADP-ribosylated proteins were not detected in HeLa cells under basal conditions, indicating that ARTD1 is more active in A2780. Moreover, we observed that A2780 cells have a significantly higher level of H_2O_2-induced ADP-ribosylated peptides compared with SKOV3 cells, which also correlated with the abundance of ARTD1 in these cells. Moreover, in both ovarian cancer cells the induction of ADP-ribosylation was observed already at 16 μM, whereas in HeLa cells ADP-ribosylatoin could be detected only at 64 μM H_2O_2. The observed concentration difference could be explained by differential expression and activation of enzymes involved in cellular ADP-ribosylation (*e.g.* different activities of PAR-degrading enzymes) or enzymes participating in the antioxidative response (*e.g.* catalases).

Because ARTD1 is the prime activated nuclear ART upon H_2O_2 treatment, the quantitative identification of ADP-ribosylated proteins allows to indirectly estimate the ARTD1 activity in the cells. Several previous studies provided a correlation between high ARTD1 expression levels and poor treatment outcome (40–42). However, certain cancer types, *e.g.* chronic leukemia, did not show the same correlation (43). Thus, to understand the role of ARTD1 in PARPi sensitivity, it is important to apply the developed analytical methods to patient tumor biopsies with high and low ARTD1 expression.

Taken together, we defined the oxidative stress-induced ADP-ribosylome for different H_2O_2 concentrations and various cell types in a qualitative and quantitative manner. The identified quantitative changes should be further validated for their predictive power as potential markers of oxidative stress conditions or as predictors of PARPi treatment outcome.

Acknowledgments—We thank Monika Fey for the expression and purification of recombinant human PARG, Michael L. Nielsen (Department of Proteomics, Novo Nordisk Foundation Center for Protein Research (NNF-CPR), University of Copenhagen, Copenhagen, Denmark) for providing the quantification SILAC data (18) used to generate supplemental Fig. S2*B* and Tobias Suter, Deena Leslie Pedrioli as well as Stephan Christen (all University of Zurich) for providing editorial assistance.

DATA AVAILABILITY

All MS raw files and Scaffold files presented in this study can be accessed at MassIVE (MSV000080334, ftp://massive.ucsd.edu/MSV000080334).

* ADP-ribosylation research in the laboratory of MOH is funded by the Swiss National Science Foundation (SNF 310030_157019) and SystemX grant (SXPHI0_141998). The authors declare no conflict of interest.

[S] This article contains supplemental material.

** To whom correspondence should be addressed: Department of Molecular Mechanisms of Disease, University of Zurich, Winterthurerstrasse 190, Zurich 8057 Switzerland. Tel.: ++41-44-635 54 74; E-mail: michael.hottiger@dmmd.uzh.ch.

REFERENCES

1. Hottiger, M. O., Hassa, P. O., Luscher, B., Schuler, H., and Koch-Nolte, F. (2010) Toward a unified nomenclature for mammalian ADP-ribosyltransferases. *Trends Biochem. Sci.* **35,** 208–219
2. Hottiger, M. O. (2016) SnapShot: ADP-ribosylation signaling. *Mol. Cell* **62,** 472
3. Luo, X., and Kraus, W. L. (2012) On PAR with PARP: cellular stress signaling through poly(ADP-ribose) and PARP-1. *Genes Dev.* **26,** 417–432
4. Andersson, A., Bluwstein, A., Kumar, N., Teloni, F., Traenkle, J., Baudis, M., Altmeyer, M., and Hottiger, M. O. (2016) PKCalpha and HMGB1 antagonistically control hydrogen peroxide-induced poly-ADP-ribose formation. *Nucleic Acids Res.* **44,** 7630–7645

Downloaded from https://www.mcponline.org by guest on November 12, 2019

5. Beck, C., Robert, I., Reina-San-Martin, B., Schreiber, V., and Dantzer, F. (2014) Poly(ADP-ribose) polymerases in double-strand break repair: focus on PARP1, PARP2 and PARP3. *Exp. Cell Res.* **329,** 18–25
6. Endres, M., Wang, Z. Q., Namura, S., Waeber, C., and Moskowitz, M. A. (1997) Ischemic brain injury is mediated by the activation of poly(ADP-ribose)polymerase. *J. Cereb. Blood Flow Metab.* **17,** 1143–1151
7. Love, S., Barber, R., and Wilcock, G. K. (1999) Increased poly(ADP-ribosyl)ation of nuclear proteins in Alzheimer's disease. *Brain* **122,** 247–253
8. Altmeyer, M., and Hottiger, M. O. (2009) Poly(ADP-ribose) polymerase 1 at the crossroad of metabolic stress and inflammation in aging. *Aging* **1,** 458–469
9. Sistigu, A., Manic, G., Obrist, F., and Vitale, I. (2016) Trial watch - inhibiting PARP enzymes for anticancer therapy. *Mol. Cell. Oncol.* **3,** e1053594
10. Farmer, H., McCabe, N., Lord, C. J., Tutt, A. N., Johnson, D. A., Richardson, T. B., Santarosa, M., Dillon, K. J., Hickson, I., Knights, C., Martin, N. M., Jackson, S. P., Smith, G. C., and Ashworth, A. (2005) Targeting the DNA repair defect in BRCA mutant cells as a therapeutic strategy. *Nature* **434,** 917–921
11. Bryant, H. E., Schultz, N., Thomas, H. D., Parker, K. M., Flower, D., Lopez, E., Kyle, S., Meuth, M., Curtin, N. J., and Helleday, T. (2005) Specific killing of BRCA2-deficient tumours with inhibitors of poly(ADP-ribose) polymerase. *Nature* **434,** 913–917
12. Drew, Y. (2015) The development of PARP inhibitors in ovarian cancer: from bench to bedside. *Br. J. Cancer* **113,** S3–S9
13. Helleday, T. (2016) PARP inhibitor receives FDA breakthrough therapy designation in castration resistant prostate cancer: beyond germline BRCA mutations. *Ann. Oncol.* **27,** 755–757
14. Lim, D., and Ngeow, J. (2016) Evaluation of the methods to identify patients who may benefit from PARP inhibitor use. *Endocr. Relat. Cancer* **23,** R267–R285
15. Martello, R., Mangerich, A., Sass, S., Dedon, P. C., and Burkle, A. (2013) Quantification of cellular poly(ADP-ribosyl)ation by stable isotope dilution mass spectrometry reveals tissue- and drug-dependent stress response dynamics. *ACS Chem. Biol.* **8,** 1567–1575
16. Zhang, Y., Wang, J., Ding, M., and Yu, Y. (2013) Site-specific characterization of the Asp- and Glu-ADP-ribosylated proteome. *Nat. Methods* **10,** 981–984
17. Jungmichel, S., Rosenthal, F., Altmeyer, M., Lukas, J., Hottiger, M. O., and Nielsen, M. L. (2013) Proteome-wide identification of poly(ADP-Ribosyl)ation targets in different genotoxic stress responses. *Mol. Cell* **52,** 272–285
18. Martello, R., Leutert, M., Jungmichel, S., Bilan, V., Larsen, S. C., Young, C., Hottiger, M. O., and Nielsen, M. L. (2016) Proteome-wide identification of the endogenous ADP-ribosylome of mammalian cells and tissue. *Nat. Commun.* **7,** 12917
19. Wolf-Yadlin, A., Hautaniemi, S., Lauffenburger, D. A., and White, F. M. (2007) Multiple reaction monitoring for robust quantitative proteomic analysis of cellular signaling networks. *Proc. Natl. Acad. Sci. U.S.A.* **104,** 5860–5865
20. Gallien, S., Duriez, E., and Domon, B. (2011) Selected reaction monitoring applied to proteomics. *J. Mass Spectrom.* **46,** 298–312
21. Peterson, A. C., Russell, J. D., Bailey, D. J., Westphall, M. S., and Coon, J. J. (2012) Parallel reaction monitoring for high resolution and high mass accuracy quantitative, targeted proteomics. *Mol. Cell. Proteomics* **11,** 1475–1488
22. Lange, V., Picotti, P., Domon, B., and Aebersold, R. (2008) Selected reaction monitoring for quantitative proteomics: a tutorial. *Mol. Syst. Biol.* **4,** 222
23. Bourmaud, A., Gallien, S., and Domon, B. (2016) Parallel reaction monitoring using quadrupole-Orbitrap mass spectrometer: Principle and applications. *Proteomics* **16,** 2146–2159
24. de Graaf, E. L., Kaplon, J., Mohammed, S., Vereijken, L. A., Duarte, D. P., Redondo Gallego, L., Heck, A. J., Peeper, D. S., and Altelaar, A. F. (2015) Signal transduction reaction monitoring deciphers site-specific PI3K-mTOR/MAPK pathway dynamics in oncogene-induced senescence. *J. Proteome Res.* **14,** 2906–2914
25. Sowers, J. L., Mirfattah, B., Xu, P., Tang, H., Park, I. Y., Walker, C., Wu, P., Laezza, F., Sowers, L. C., and Zhang, K. (2015) Quantification of histone modifications by parallel-reaction monitoring: a method validation. *Anal. Chem.* **87,** 10006–10014
26. Shi, T., Gao, Y., Gaffrey, M. J., Nicora, C. D., Fillmore, T. L., Chrisler, W. B., Gritsenko, M. A., Wu, C., He, J., Bloodsworth, K. J., Zhao, R., Camp, D. G., 2nd, Liu, T., Rodland, K. D., Smith, R. D., Wiley, H. S., and Qian, W. J. (2015) Sensitive targeted quantification of ERK phosphorylation dynamics and stoichiometry in human cells without affinity enrichment. *Anal. Chem.* **87,** 1103–1110
27. Tsuchiya, H., Tanaka, K., and Saeki, Y. (2013) The parallel reaction monitoring method contributes to a highly sensitive polyubiquitin chain quantification. *Biochem. Biophys. Res. Commun.* **436,** 223–229
28. Kistemaker, H. A., Nardozza, A. P., Overkleeft, H. S., van der Marel, G. A., Ladurner, A. G., and Filippov, D. V. (2016) Synthesis and macrodomain binding of mono-ADP-ribosylated peptides. *Angew Chem. Int. Ed. Engl.* **55,** 10634–10638
29. Deleted in proof.
30. Rosenthal, F., Nanni, P., Barkow-Oesterreicher, S., and Hottiger, M. O. (2015) Optimization of LTQ-Orbitrap Mass Spectrometer Parameters for the Identification of ADP-Ribosylation Sites. *J. Proteome Res.* **14,** 4072–4079
31. Bilan, V., Leutert, M., Nanni, P., Panse, C., and Hottiger, M. O. (2016) Combining HCD and EThcD fragmentation in a product dependent-manner confidently assigns proteome-wide ADP-ribose acceptor sites. *Analytical chemistry* **89,** 1523–1530
32. Rosenberger, G., Koh, C. C., Guo, T., Rost, H. L., Kouvonen, P., Collins, B. C., Heusel, M., Liu, Y., Caron, E., Vichalkovski, A., Faini, M., Schubert, O. T., Faridi, P., Ebhardt, H. A., Matondo, M., Lam, H., Bader, S. L., Campbell, D. S., Deutsch, E. W., Moritz, R. L., Tate, S., and Aebersold, R. (2014) A repository of assays to quantify 10,000 human proteins by SWATH-MS. *Scientific Data* **1,** 140031,
33. Fahrer, J., Kranaster, R., Altmeyer, M., Marx, A., and Burkle, A. (2007) Quantitative analysis of the binding affinity of poly(ADP-ribose) to specific binding proteins as a function of chain length. *Nucleic Acids Res.* **35,** e143
34. Wahlberg, E., Karlberg, T., Kouznetsova, E., Markova, N., Macchiarulo, A., Thorsell, A. G., Pol, E., Frostell, A., Ekblad, T., Oncu, D., Kull, B., Robertson, G. M., Pellicciari, R., Schuler, H., and Weigelt, J. (2012) Family-wide chemical profiling and structural analysis of PARP and tankyrase inhibitors. *Nat. Biotechnol.* **30,** 283–288
35. Tabb, D. L., Vega-Montoto, L., Rudnick, P. A., Variyath, A. M., Ham, A. J., Bunk, D. M., Kilpatrick, L. E., Billheimer, D. D., Blackman, R. K., Cardasis, H. L., Carr, S. A., Clauser, K. R., Jaffe, J. D., Kowalski, K. A., Neubert, T. A., Regnier, F. E., Schilling, B., Tegeler, T. J., Wang, M., Wang, P., Whiteaker, J. R., Zimmerman, L. J., Fisher, S. J., Gibson, B. W., Kinsinger, C. R., Mesri, M., Rodriguez, H., Stein, S. E., Tempst, P., Paulovich, A. G., Liebler, D. C., and Spiegelman, C. (2010) Repeatability and reproducibility in proteomic identifications by liquid chromatography-tandem mass spectrometry. *J. Proteome Res.* **9,** 761–776
36. Stordal, B., Timms, K., Farrelly, A., Gallagher, D., Busschots, S., Renaud, M., Thery, J., Williams, D., Potter, J., Tran, T., Korpanty, G., Cremona, M., Carey, M., Li, J., Li, Y., Aslan, O., O'Leary, J. J., Mills, G. B., and Hennessy, B. T. (2013) BRCA1/2 mutation analysis in 41 ovarian cell lines reveals only one functionally deleterious BRCA1 mutation. *Mol. Oncol.* **7,** 567–579
37. Jwa, M., and Chang, P. (2012) PARP16 is a tail-anchored endoplasmic reticulum protein required for the PERK- and IRE1alpha-mediated unfolded protein response. *Nat. Cell Biol.* **14,** 1223–1230
38. Fabrizio, G., Di Paola, S., Stilla, A., Giannotta, M., Ruggiero, C., Menzel, S., Koch-Nolte, F., Sallese, M., and Di Girolamo, M. (2015) ARTC1-mediated ADP-ribosylation of GRP78/BiP: a new player in endoplasmic-reticulum stress responses. *Cell Mol. Life Sci.* **72,** 1209–1225
39. Li, M., and Yu, X. (2013) Function of BRCA1 in the DNA damage response is mediated by ADP-ribosylation. *Cancer Cell* **23,** 693–704
40. Noren Hooten, N., Kompaniez, K., Barnes, J., Lohani, A., and Evans, M. K. (2011) Poly(ADP-ribose) polymerase 1 (PARP-1) binds to 8-oxoguanine-DNA glycosylase (OGG1). *J. Biol. Chem.* **286,** 44679–44690
41. Dantzer, F., de La Rubia, G., Menissier-De Murcia, J., Hostomsky, Z., de Murcia, G., and Schreiber, V. (2000) Base excision repair is impaired in mammalian cells lacking Poly(ADP-ribose) polymerase-1. *Biochemistry* **39,** 7559–7569
42. Molden, R. C., Bhanu, N. V., LeRoy, G., Arnaudo, A. M., and Garcia, B. A. (2015) Multi-faceted quantitative proteomics analysis of histone H2B isoforms and their modifications. *Epigenetics Chromatin* **8,** 15
43. Bungard, D., Fuerth, B. J., Zeng, P. Y., Faubert, B., Maas, N. L., Viollet, B., Carling, D., Thompson, C. B., Jones, R. G., and Berger, S. L. (2010) Signaling kinase AMPK activates stress-promoted transcription via histone H2B phosphorylation. *Science* **329,** 1201–1205

Downloaded from https://www.mcponline.org by guest on November 12, 2019